Available online at www.sciencedirect.com

ScienceDirect

Energy Procedia 76 (2015) 600 – 606

Energy Procedia

European Geosciences Union General Assembly 2015, EGU

Division Energy, Resources & Environment, ERE

Caprock permeabilities must be considered in assessments of ground surface displacements in geological underground utilization

Thomas Kempka*, Elena Tillner

GFZ German Research Centre for Geosciences, Section 5.3 – Hydrogeology, Telegrafenberg, 14473 Potsdam, Germany

Abstract

Ground surface displacements resulting from geological underground utilization may induce serious damages to surface infrastructure. We carried out coupled hydro-mechanical simulations to compare the impact of caprock permeability on vertical displacements at a storage reservoir top and the ground surface. A 3D numerical scenario analysis was employed to assess the effects of caprock permeabilities equal to zero and varied between 10^{-20} m^2 and 10^{-16} m^2. Simulation results show that vertical ground surface displacements almost double with each order of magnitude increase in caprock permeability and that vertical ground surface displacements are generally higher than those observed at the reservoir top.

Peer-review under responsibility of the GFZ German Research Centre for Geosciences

Keywords: Caprock permeability; ground surface displacements; reservoir utilization; hydro-mechanical modeling; numerical simulation

1. Introduction

Coupled hydro-mechanical simulations carried out for the assessment of vertical ground surface displacements, which generally accompany fluid production from and storage in geological reservoirs, are often calculated without consideration of fluid flow processes occurring in the caprock sequences [1-10]. The reasons for applying this

* Corresponding author. Tel.: +49-331-288-1865.
E-mail address: kempka@gfz-potsdam.de

Peer-review under responsibility of the GFZ German Research Centre for Geosciences
doi:10.1016/j.egypro.2015.07.878

simplification are mainly associated with the computational efficiency of a coupled hydro-mechanical model, but may also result from limitations of the applied hydraulic simulators, e.g., maximum number of elements and nodes applicable for a sufficiently accurate representation of non-isothermal flow processes across great model thicknesses. Generally, ground surface displacements may trigger damage of surface infrastructure such as pipelines, roads and buildings, depending on the resulting differential displacements in the affected area, whereby the allowable thresholds depend on the evaluated structure [11].

Tillner et al. [12] demonstrated that different assumptions made on caprock permeability in coupled hydro-mechanical modeling by two independent modeling groups can result in significant deviations between the simulation results, especially when considering the calculated vertical ground surface displacements. Further, they found that ground surface displacements were higher in their simulation study compared to those observed at the reservoir top of an on-shore CO_2 storage site. Considering these findings, we decided to have a more detailed investigation on the role of caprock permeability in coupled hydro-mechanical simulations and employed a scenario analysis based on fully coupled 3D hydro-mechanical modeling. For that purpose, a synthetic 3D model was implemented comprising two reservoir and caprock units, respectively, whereby the permeability of both caprocks was varied by one magnitude with each simulation scenario in a range between 10^{-20} m^2 and 10^{-16} m^2, which is documented to be representative for reservoir caprocks by different authors [e.g. 13-28]. In addition, we conducted a simulation with a caprock permeability of zero, representing the standard modeling procedure chosen in many hydro-mechanical simulations.

2. Hydro-mechanical model geometry and parameterization

2.1. 3D model geometry

The implemented 3D model considers five geological formations including two aquifers (primary and secondary reservoir) and three aquicludes (caprocks and model basement) as shown in Fig. 1. A quarter model of a hypothetic anticline system with a total extent of 20 km x 20 km was employed taking into account the existing symmetry. The depth of the primary reservoir top is 1,000 m at the location of the anticline top and 1,500 m at a distance of 10 km, assuming a radial anticline dip of 2.86°. The thicknesses at the location of the vertical injection well are 50 m for the primary reservoir, 200 m for the intermediate caprock, 25 m for the secondary reservoir and 775 m for the upper caprock, respectively.

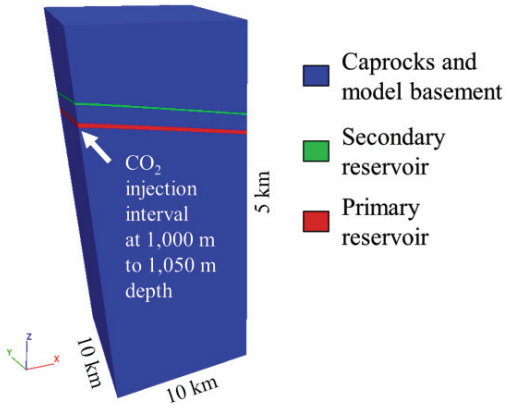

Fig. 1. Quarter-symmetric numerical model of a synthetic anticline applied in the present study.

Horizontal model discretization is 10 km x 10 km, using a tartan type grid to ensure a sufficient resolution in the near-wellbore area, with increasing element sizes towards the lateral model boundaries. A tartan grid type is also applied in vertical direction to ensure a sufficient discretization of the single geological units.

2.2. Mechanical parameters

Mechanical parameters assigned to the geological units are derived from literature data summarized by Tillner et al. [12], while the hydrodynamic flow model data is parameterized using data from Kempka and Kühn [29]. The porosity sensitivity exponent is derived from David et al. [30].

Table 1. Parameters assigned to the geological formations in the hydro-mechanical model [12, 29-30].

Property	Upper caprock	Secondary reservoir	Intermediate caprock	Primary reservoir	Model basement
Young's modulus (GPa)	19.9	26.0	31.0	27.7	60.0
Poisson's coefficient (-)	0.24	0.18	0.29	0.26	0.19
Friction angle (°)	20	23	20	25	30
Cohesion and Tensile strength (MPa)			5		
Dilation angle (°)			0		
Density (kg/m³)	2,650	2,658	2,362	2,453	2,698
Biot's coefficient (-)			1		
Porosity (-)	0.02	0.2	0.02	0.17	0.1
Permeability (m^2)	variable	2×10^{-13}	variable	4×10^{-13}	variable
van Genuchten $1/P_0$ (Pa^{-1})	1.77×10^{-7}	7.91×10^{-5}	1.77×10^{-7}	1.21×10^{-4}	1.77×10^{-7}
van Genuchten λ (-)			0.65		
Porosity sensitivity exponent (-)	5	20	5	20	5

2.3. Hydro-mechanical boundary and initial conditions

We assigned constant velocities of zero displacement perpendicular to the lateral and bottom model boundaries, and allowed displacements in any direction at the upper model boundary. A normal faulting stress regime with $S_H = 0.85\ S_V$ was assigned to the mechanical model with the horizontal total stress S_H and vertical total stress S_V. However, it should be noted that the stress regime has a rather negligible impact on displacements in the absence of fault reactivation [31]. The hydrodynamic model is determined by Dirichlet conditions at the top and lateral boundaries in radial direction, while the tangential model boundaries have Neumann 'no flow' conditions assigned. Temperature is assigned with a geothermal gradient of 0.03 K/m, while pore pressure is determined by atmospheric conditions at the ground surface. The primary and secondary reservoirs exhibit salinities of 25 % and 20 % by weight, respectively, whereas all caprocks do not comprise any salt mass fraction to allow for using salt to act as a tracer. However, this is not further addressed in the present manuscript. An iterative pore pressure calculation over the entire model depth based on the assigned pressure and temperature conditions was carried out using the equation of state of Rowe and Chou [32] in advance of the equilibration run undertaken with the TOUGH2-MP/ECO2N [33-34] simulator. The FLAC^{3D} simulator [35] was applied to calculate the mechanical equilibrium based on the

elastoplastic Mohr-Coulomb constitutive law before initiation of the hydro-mechanical coupling. Then, the hydro-mechanical simulations were carried out, using pore pressure and volumetric strain increments as coupling parameters in between previously specified iteration intervals. Based on the given volumetric strain increments, porosity and permeability changes in the hydrodynamic simulation models were updated by application of the relationship introduced by Chin et al. [36].

2.4. Injection schedule and investigated scenarios

A total amount of 34 Mt CO_2 is injected into the primary reservoir at the top of the anticline as applied by Tillner et al. [37] for a similar, but realistic geological setting, represented by a constant injection rate of 13.48 kg/s in the quarter domain model used here. This rate is maintained for a time of 20 years, and then followed by a post-injection period of another 20 years. A caprock permeability of zero is assumed in the reference scenario, while caprock permeabilities of 10^{-16} m^2, 10^{-17} m^2, 10^{-18} m^2, 10^{-19} m^2 and 10^{-20} m^2 were applied in the other five scenarios considered in the present study. Any other parameters are not changed in the six coupled hydro-mechanical simulation runs.

3. Hydro-mechanical simulation results

Fig. 2 shows the bottomhole pressure (BHP) development in time for different caprock permeabilities at the reservoir top. The maximum increase in BHP occurs after the start of the CO_2 injection, whereby maximum values are almost identical for all scenarios at that time. At the end of the injection period, variations in BHP of up to 0.4 MPa are observed, decreasing to about 0.3 MPa at the end of the simulation runs (40 years). Considering a caprock permeability of 10^{-16} m^2 does not induce a pore pressure increase between the maximum pressure peak occurring directly after the start of injection and the end of injection (20 years), as observed for all other scenarios. Nevertheless, caprock permeability shows only negligible impact on pressure build-up with open lateral boundaries.

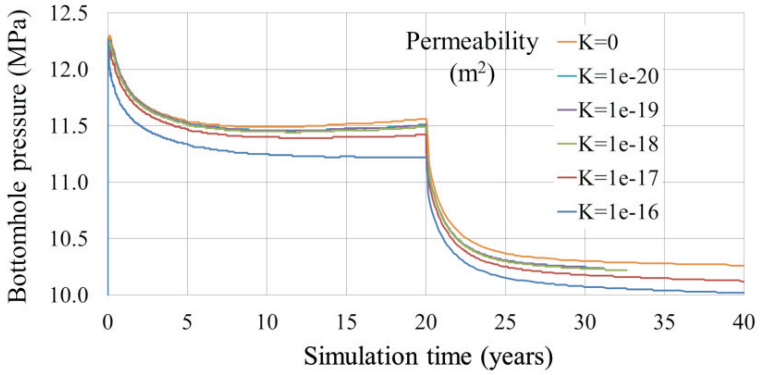

Fig. 2. Bottomhole pressure (BHP) at primary reservoir top as a function of time and caprock permeability (in m^2). Maximum increase in BHP at the start of injection is almost identical for all investigated scenarios, whereby BHP decreases with increasing caprock permeability and is not starting to increase again after 20 years of simulation in the K = 1 x 10^{-16} m^2 case.

Vertical displacements at the top of the primary reservoir and at the ground surface are plotted in Fig. 3. Simulation results demonstrate that in all cases, expect in the scenario with a caprock permeability of zero, vertical displacements at the ground surface are generally higher than those observed at the primary reservoir top. This behavior is also achieved for caprock permeabilities of 10^{-20} m^2 to 10^{-18} m^2 after about three years, one year and a few months after the start of injection, respectively. Further, vertical displacements are increased by about one magnitude with an increase in caprock permeability from 10^{-20} m^2 to 10^{-16} m^2, and generally double with each order of magnitude increase in caprock permeability.

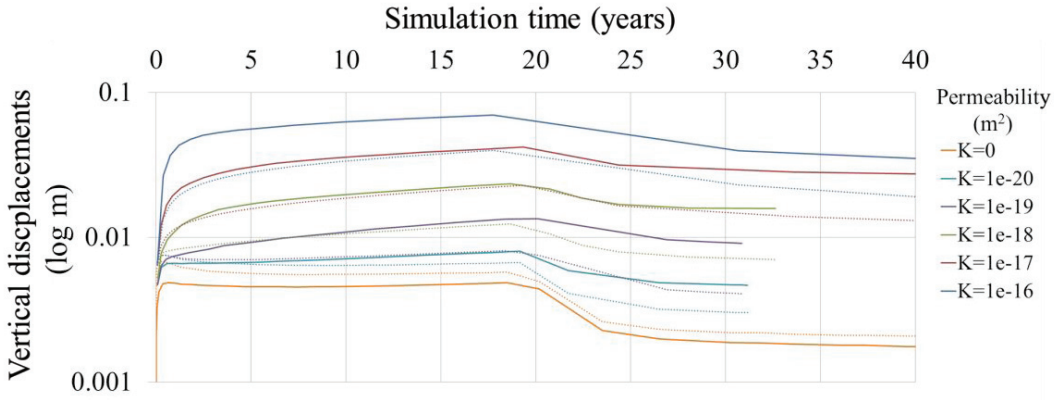

Fig. 3. Vertical displacements at the primary reservoir top (dotted lines) and at the ground surface (solid lines) for all investigated scenarios (caprock permeabilities are given in m^2). Scenarios with $K = 10^{-16}$ m^2 and $K = 10^{-17}$ m^2 exhibit higher displacements at the ground surface than at the primary reservoir top at any time of simulation, while this behaviour develops first after a couple of months to years in the $K = 10^{-18}$ m^2 to $K = 10^{-20}$ m^2 scenarios. Vertical displacements at the primary reservoir top are always higher than those at the ground surface in the zero caprock permeability scenario.

4. Discussion and conclusions

Ground surface displacements resulting from geological underground utilization may induce surface infrastructure damage, if exposing a spatial differential character. In the present study, we carried out coupled hydro-mechanical simulations to assess the impact of caprock permeability on vertical displacements at the top of a storage reservoir and the ground surface. By employing a 3D numerical scenario analysis, we investigated the effects of caprock permeabilities set to zero as well as varied between 10^{-20} m^2 and 10^{-16} m^2. Our simulation results demonstrate that pore pressure in the reservoir is not notably influenced by varying caprock permeabilities, if the hydrodynamic model boundaries are defined as open to fluid flow. However, vertical ground surface displacements almost double with each order of magnitude increase in caprock permeability and vertical ground surface displacements are generally higher than those observed at the reservoir top.

At the In Salah CO_2 storage site in Algeria, Rutqvist et al. [26] observed a higher vertical uplift at the reservoir top (1.6 cm) than at the ground surface (1.2 cm) in their hydro-mechanical simulations, assuming a caprock permeability of 10^{-21} m^2. The authors also demonstrated that a caprock permeability of 10^{-19} m^2 increases the maximum ground surface uplift by 0.8 cm due to fluid migration into the caprock, resulting in higher displacements at the ground surface than at the reservoir top. This supports the results achieved in the present study, but also that a permeability threshold of relevance for the assessment of ground surface displacements in underground utilization may exist for caprock permeabilities between 10^{-21} m^2 and 10^{-20} m^2. Even though, the injection depth at In Salah is about 800 m deeper than that used in the present study, we intend to continue investigating the relevance of a potential caprock permeability threshold in an upcoming hydro-mechanical simulation study.

The results of the present study emphasize that caprock permeabilities must be taken into account in coupled hydro-mechanical simulations of underground utilization in order not to underestimate ground surface displacements, whereby the choice of the permeability magnitude has significant implications for the calculated vertical displacements.

References

[1] Kempka T, Klapperer S, Norden B. Coupled hydro-mechanical simulations demonstrate system integrity at the Ketzin pilot site for CO_2 storage. Rock Engineering and Rock Mechanics: Structures in and on Rock-Masses Proceeding of EUROCK 2014, ISRM European Regional Symposium, p. 1317-1322.

[2] Klimkowski L, Nagy S, Papiernik B, Orlic B, Kempka T. Numerical Simulations of Enhanced Gas Recovery at the Załęcze Gas Field in Poland Confirm High CO_2 Storage Capacity and Mechanical Integrity. Oil Gas Sci Technol 2015; in press. doi: 10.2516/ogst/2015012.

[3] Magri F, Tillner E, Wang W, Watanabe N, Zimmermann G, Kempka T. 3D Hydro-mechanical Scenario Analysis to Evaluate Changes of the Recent Stress Field as a Result of Geological CO_2 Storage. Energy Procedia 2013; 40: 375-383. doi.org/10.1016/j.egypro.2013.08.043.
[4] Orlic B, Mazurowski M, Papiernik B, Nagy S. Assessing the geomechanical effects of CO_2 injection in a depleted gas field in Poland by field scale modelling. Proceedings of EUROCK 2013 - The 2013 ISRM International Symposium, Kwaśniewski M., Łydżba D. (eds), Wrocław, 21-26 Sept., London, Taylor & Francis Group, 969-975.
[5] Ouellet A, Bérard T, Desroches J, Frykman P, Welsh P, Minton J, Pamukcu J, Hurter S, Schmidt-Hattenberger C. Reservoir geomechanics for assessing containment in CO_2 storage: A case study at Ketzin, Germany. Energy Procedia 2011; 4: 3298-3305.
[6] Röhmann L, Tillner E, Magri F, Kühn M, Kempka T. Fault Reactivation and Ground Surface Uplift Assessment at a Prospective German CO_2 Storage Site. Energy Procedia 2013; 40: 437-446. doi:10.1016/j.egypro.2013.08.050.
[7] Shi J-Q, Smith J, Durucan S, Korre A. A coupled reservoir simulation-geomechanical modelling study of the CO_2 injection-induced ground surface uplift observed at Krechba, In Salah. Energy Procedia 2013; 37: 3719-3726.
[8] Tenthorey E, Vidal-Gilbert S, Backé G, Puspitasari R, Pallikathekathil ZJ, Maney B, Dewhurst D. Modelling the geomechanics of gas storage: A case study from the Iona gas field, Australia. Int J Greenh Gas Con 2013; 13: 138-148.
[9] Shi J-Q, Durucan S. A coupled reservoir-geomechanical simulation study of CO_2 storage in a nearly depleted natural gas reservoir. Energy Procedia 2009; 1(1): 3039-3046.
[10] Vidal-Gilbert S, Nauroy J-F, Brosse E. 3D geomechanical modelling for CO_2 geologic storage in the Dogger carbonates of the Paris Basin. Int J Greenh Gas Con 2009; 3: 288-299.
[11] Bjerrum L. Allowable settlements of structures. Norw. Geot. Inst., Oslo 98, 1973.
[12] Tillner E, Shi J-Q, Bacci G, Nielsen CM, Frykman P, Dalhoff F, Kempka T. Coupled Dynamic Flow and Geomechanical Simulations for an Integrated Assessment of CO_2 Storage Impacts in a Saline Aquifer. Energy Procedia 2014; 63: 2879-2893. doi:10.1016/j.egypro.2014.11.311.
[13] Huang Z-Q, Winterfeld PH, Xiong Y, Wu Y-S, Yao J. Parallel simulation of fully-coupled thermal-hydro-mechanical processes in CO_2 leakage through fluid-driven fracture zones. Int J Greenh Gas Con 2015; 34: 39-51. doi:10.1016/j.ijggc.2014.12.012.
[14] Kim S, Hosseini SA. Hydro-thermo-mechanical analysis during injection of cold fluid into a geologic formation. Int J Rock Mech Min 2015; 77: 220-236.
[15] Zhang Y, Langhi L, Schaubs PM, Delle Piane C, Dewhurst DN, Stalker L, Michael K. Geomechanical stability of CO_2 containment at the South West Hub Western Australia: A coupled geomechanical–fluid flow modelling approach. Int J Greenh Gas Con 2015; 37: 12-23.
[16] Mbia EN, Frykman P, Nielsen CM, Fabricius IL, Pickup GE, Bernstone C. Caprock compressibility and permeability and the consequences for pressure development in CO_2 storage sites. Int J Greenh Gas Con 2014; 22: 139-153.
[17] Rinaldi AP, Rutqvist J, Cappa F. Geomechanical effects on CO_2 leakage through fault zones during large-scale underground injection. Int J Greenh Gas Cont 2014; 20: 117-131.
[18] Vilarrasa V, Olivella S, Carrera J, Rutqvist J. Long term impacts of cold CO_2 injection on the caprock integrity, Int J Greenh Gas Con 2014; 24: 1-13.
[19] Zhou L, Hou MZ, Gou Y, Li M. Numerical investigation of a low-efficient hydraulic fracturing operation in a tight gas reservoir in the North German Basin. J Petrol Sci Eng 2014; 120: 119-129.
[20] Rinaldi AP, Rutqvist J. Modeling of deep fracture zone opening and transient ground surface uplift at KB-502 CO_2 injection well, In Salah, Algeria. Int J Greenh Gas Con 2013; 12: 155-167.
[21] Vilarrasa V, Silva O, Carrera J, Olivella S. Liquid CO_2 injection for geological storage in deep saline aquifers. Int J Greenh Gas Con 2013; 14: 84-96.
[22] Vilarrasa V, Carrera J, Olivella S. Hydromechanical characterization of CO_2 injection sites. Int J Greenh Gas Con 2013; 19: 665-677. doi:10.1016/j.ijggc.2012.11.014.
[23] Yamamoto S, Miyoshi S, Sato S, Suzuki K. Study on Geomechanical Stability of the Aquifer-caprock System During CO_2 Sequestration by Coupled Hydromechanical Modelling. Energy Procedia 2013; 37: 3989-3996.
[24] Cappa F, Rutqvist J. Modeling of coupled deformation and permeability evolution during fault reactivation induced by deep underground injection of CO_2. Int J Greenh Gas Con 2011; 5(2): 336-346.
[25] Vilarrasa V, Olivella S, Carrera S. Geomechanical stability of the caprock during CO_2 sequestration in deep saline aquifers. Energy Procedia 2011; 4: 5306-5313.
[26] Rutqvist J, Vasco DW, Myer L. Coupled reservoir-geomechanical analysis of CO_2 injection and ground deformations at In Salah, Algeria. Int J Greenh Gas Con 2010; 4: 225-230.
[27] Vilarrasa V, Bolster D, Olivella S, Carrera S. Coupled hydromechanical modeling of CO_2 sequestration in deep saline aquifers. Int J Greenh Gas Con 2010; 4(6): 910-919.
[28] Rutqvist J, Birkholzer J, Cappa F, Tsang C-F. Estimating maximum sustainable injection pressure during geological sequestration of CO_2 using coupled fluid flow and geomechanical fault-slip analysis. Energ Convers Manage 2007; 48(6): 1798-1807.
[29] Kempka T, Kühn M. Numerical simulations of CO_2 arrival times and reservoir pressure coincide with observations from the Ketzin pilot site, Germany. Environ Earth Sci 2013; 70(8), 3675-3685. doi:10.1007/s12665-013-2614-6.
[30] David C, Wong T-F, Zhu W, Zhang J. Laboratory measurements of compaction-induced permeability change in porous rocks: Implications for the generation and maintenance of pore pressure excess in the crust. Pure Appl Geophys 1994; 143 (1-3): 425-456.
[31] Kempka T, Nielsen CM, Frykman P, Shi JQ, Bacci G, Dalhoff F. Coupled Hydro-Mechanical Simulations of CO_2 Storage Supported by Pressure Management Demonstrate Synergy Benefits from Simultaneous Formation Fluid Extraction. Oil Gas Sci Technol 2015; in press. doi:10.2516/ogst/2014029.
[32] Rowe AM, Chou JCS. Pressure-Volume-Temperature-Concentration Relation of Aqueous NaCl Solutions. J Chem Eng Data 1970; 15(1): 61-66.

[33] Pruess K. ECO2N: a TOUGH2 fluid property module for mixtures of water, NaCl, and CO_2. Report LBNL-57952, Lawrence Berkeley National Laboratory, Berkeley. 2005.
[34] Zhang K, Wu Y-S, Pruess K (2008) User's guide for TOUGH2-MP - a massively parallel version of the TOUGH2 code. Report LBNL-315E, Earth Sciences Division, Lawrence Berkeley, National Laboratory, Berkeley. 2008.
[35] Itasca Consulting Group, Inc. Advanced Three-Dimensional Continuum Modelling for Geotechnical Analysis of Rock, Soil and Structural Support. In FLAC3D Software Version 5.0. User's Manual; Itasca Consulting Group, Inc.: Minneapolis, MN, USA, 2014.
[36] Chin LY, Raghavan R, Thomas LK. Fully coupled geomechanics and fluidflow analysis of wells with stress-dependent permeability. SPE J. 2000; 5: 32–45.
[37] Tillner E, Kempka T, Nakaten B, Kühn M. Brine migration through fault zones: 3D numerical simulations for a prospective CO_2 storage site in Northeast Germany. Int J Greenh Gas Con 2013; 19: 689-703. doi:/10.1016/j.ijggc.2013.03.012.